
Autoencoding Conditional Neural Processes for Representation Learning

Victor Prokhorov*
School of Informatics
University of Edinburgh

Ivan Titov
School of Informatics
University of Edinburgh

N. Siddharth
School of Informatics
University of Edinburgh
The Alan Turing Institute

Abstract

Conditional neural processes (CNPs) are a flexible and efficient family of models that *learn to learn* a stochastic process from observations. In the visual domain, they have seen particular application in contextual image completion—observing pixel values at some locations to predict a distribution over values at other unobserved locations. However, the choice of pixels in learning such a CNP is typically either random or derived from a simple statistical measure (e.g. pixel variance). Here, we turn the problem on its head and ask: which pixels would a CNP like to observe? That is, which pixels allow fitting CNP, and do such pixels tell us something about the underlying image? Viewing the context provided to the CNP as fixed-size latent representations, we construct an amortised variational framework, Partial Pixel Space Variational Autoencoder (PPS-VAE), for predicting this context simultaneously with learning a CNP. We evaluate PPS-VAE on a set of vision datasets, and find that not only is it possible to learn context points while also fitting CNPs, but that their spatial arrangement and values provides strong signal for the information contained in the image—evaluated through the lens of classification. We believe the PPS-VAE provides a promising avenue to explore learning interpretable and effective visual representations.²

1 Introduction

Conditional neural processes [Garnelo et al., 2018a, CNPs] are a family of models that learn distribution over functions. In contrast to conventional approaches such as Gaussian processes, which are effective but become computationally expensive once the data size increases, CNPs are both flexible regarding the functions they approximate, thanks to neural networks, and scalable to large datasets. In the visual domain, they have been used for contextual image completion. Given a context set, a set of ordered pairs—observed pixel values and their image coordinates—CNPs learn to impute the other, unobserved, pixels.

While prior work on CNPs primarily focusses on model choices such as inductive biases that allow capturing various properties of the context set better [Gordon et al., 2020] or dependencies between the unobserved pixel values [Garnelo et al., 2018b], we explore a key *dual* question—regarding the context set itself. Where the context set is typically chosen at random to train the CNP, we ask: *which pixels would a CNP like to observe?* That is, which pixels allow fitting the CNP, and do such pixels tell us something about the underlying image? We answer these questions by casting

*mail to: vprokhorov@exceed.ed.ac.uk

²link to the code: soon will be added

them in the frame of representation learning, where the chosen context set can be viewed as a *latent* representations of the image—one that happens to exist in the data space.

From a purely representation-learning perspective, one can relate the question above with that of learning a discrete latent ‘code’, as first established in [van den Oord et al., 2017, VQ-VAE], and subsequently popularised by approaches like DALL-E [Ramesh et al., 2021]. Compared to the VQ-VAE approach, here the discrete ‘code’ directly corresponds to a sparse set of image pixels that faithfully captures its contents, as measured by its ability to impute the remaining pixels, with the benefit that the arrangement of pixels and its values are *interpretable by construction* — it has 1-1 correspondence with the data. Given the interpretation of our model as *imputing* the remainder of the observation from the given pixel ‘codebook’, we bring together the ideas of discrete representation learning and learning-to-learn stochastic processes (CNPs) into a single framework—the partial pixel specification variational autoencoder (PPS-VAE, shown in Figure 1).

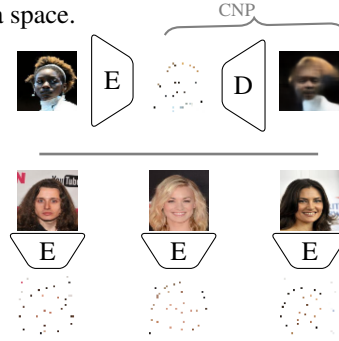


Figure 1: (top) The PPS-VAE framework. (bottom) Examples of meaningful context points induced by the encoder.

Specifically, our contributions in this work are:

- a framework (PPS-VAE) that uses amortised variational inference to *learn to predict* context points that a CNP can faithfully complete,
- ablation to identify the effect of learning to predict context points sequentially or independently,
- qualitative and quantitative evaluation over different image datasets—FashionMNIST [Xiao et al., 2017], CIFAR10 [Krizhevsky and Hinton, 2009] and CelebA [Liu et al., 2015],
- showing that the context points learnt by the PPS-VAE encode useful information in their pattern and values—evaluated through both qualitative observation and a classification-probe task, and
- demonstrating that the model learns to faithfully characterise the dataset by evaluating its ability to perform *unconditional* generation—something that the VQ-VAE family of approaches needs additional training and fitting for.

2 Model

CNPs: Given a predictor function $f : \mathcal{X} \rightarrow \mathcal{Y}$ that maps observations $x \in \mathcal{X}$ to targets $y \in \mathcal{Y}$, and a *context set* $\mathcal{C} = \{(x_m, y_m)\}_{m=1}^M$, a CNP [Garnelo et al., 2018a] learns a distribution over functions $f(x; \mathcal{C})$ —predicting targets conditioned on the context set \mathcal{C} . For unseen observations $\mathbf{x}_T = \{x_t\}_{t=1}^T$, the CNP defines the distribution over targets $\mathbf{y}_T = \{y_t\}_{t=1}^T$ as

$$p_\theta(\mathbf{y}_T | \mathbf{x}_T, \mathcal{C}) = \prod_{t=1}^T \mathcal{N}(y_t | \mu_t, \sigma_t), \text{ where } \mu_t, \sigma_t = s_\theta(x_t, r_\theta(\mathcal{C})). \quad (1)$$

Crucially, it relies on transforming the entire context set \mathcal{C} in a permutation-invariant fashion [Zaheer et al., 2017, DeepSet] using r_θ , to construct the parameters of the distribution through s_θ , using neural networks as parameters.

In the image domain, a CNP learns to predict the colour values \mathbf{y}_T at unseen locations \mathbf{x}_T given a set of observed pixel locations \mathbf{x}_M and their corresponding values \mathbf{y}_M . By observing *some* small, sparse subset of the image itself, the task here is to impute the rest of the image. Note that, in this setting, knowing the set of observed locations \mathbf{x}_M implies knowing the set of unseen locations \mathbf{x}_T , as for images of fixed size, one is the complement ($\mathbf{x}_T = \mathbf{x}_M'$) of the other. Learning a CNP in this setting involves (random) sampling of different context sets and subsequent imputation of the values at unseen locations, across a dataset of images.

Autoencoding CNPs: To answer our motivating question of what kinds of context sets the CNP would like to observe, and how meaningful these sets of points are, we first need to cast the CNP as a fully generative model as shown in Figure 2a (left),

$$p_\theta(\mathbf{x}, \mathbf{y} | M) = p_\theta(\mathbf{x}_M) p_\theta(\mathbf{y}_M | \mathbf{x}_M) p_\theta(\mathbf{y}_T | \mathbf{x}_T, \mathbf{x}_M, \mathbf{y}_M).$$

Here, M is taken to be a given fixed value, $p_\theta(\mathbf{x}_M)$ defines a distribution over *arrangements* of M pixel locations in an image, and $p_\theta(\mathbf{y}_M | \mathbf{x}_M)$ a distribution over values at the given locations. The

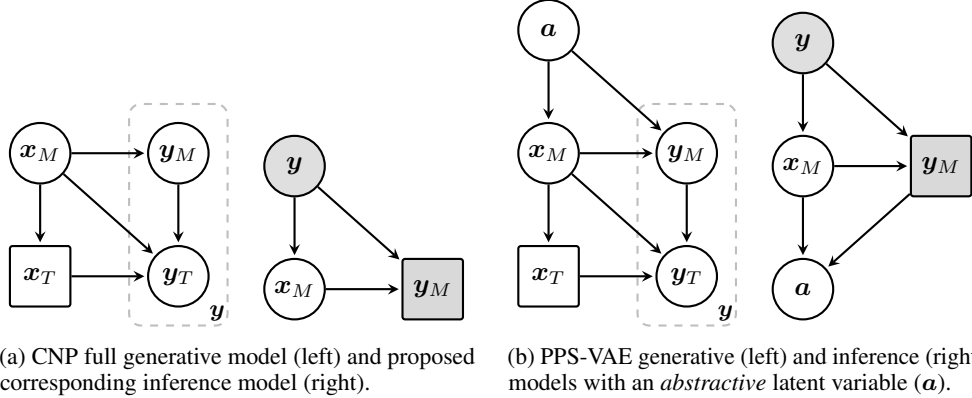


Figure 2: A comparison of the generative and inference models for the CNP and PPS-VAE.

model can be viewed as generating data in two stages (autoregressive): first generating the values corresponding to the context points, and subsequently, conditioning on these locations and values to impute the values elsewhere on the image.

Where the standard CNP formulation estimates the marginal $p_\theta(\mathbf{y}|M)$ by sampling uniformly at random from $p(\mathbf{x}_M)$, one can instead construct a more informative importance-sampled estimator by employing a variational posterior $q_\phi(\mathbf{x}_M|\mathbf{y}, M)$ in the vein of [Kingma and Welling, 2014, VAE]. Crucially, given a means to generate the pixel locations \mathbf{x}_M , one can simply perform a lookup in the given image \mathbf{y} at those locations to derive \mathbf{y}_M —viewed as an observation in itself—as shown in Figure 2a (right).

In this setting, from a representation-learning perspective, the context set can be seen as a *partial pixel specification* (PPS) of the given complete image, which leads us to term this family of models as PPS-VAE(s). However, before formally defining the model and learning objective, there are a couple of features worth highlighting and expanding upon.

Inductive biases: In the first instance, given our focus on the visual domain, we employ a specific variant of CNPs called the ConvCNP [Gordon et al., 2020], which explicitly incorporates translation equivariance and locality constraints enforced by convolutional neural network (CNN) filters. For our inference model $q_\phi(\mathbf{x}_M|\mathbf{y}, M)$, we complement this inductive bias in the CNP by using CNNs again. We find this to be an important design decision, as attempting to model these components using the standard multi-layer perceptron (MLP) [as in Garnelo et al., 2018a] causes a number of issues, primarily to do with the model seeking to use the context set/PPS simply as a generic lookup table, with little to no spatial meaning or relevance (see Appendix I for qualitative results). The CNN-based setup provides the requisite inductive bias that allows meaningful spatial arrangement of points, reflective of the image (see Section 3.3)

Abstractive PPS-VAE: In the model described previously (Figure 2a), the generative model includes a conditional distribution $p_\theta(\mathbf{y}_M|\mathbf{x}_M)$ whose role is to process a set of image pixel locations and identify what values they ought to express. Given that the distribution of values in a pixel can vary enormously depending on the context provided by values at other (both global and local) locations, a single parametric function (in the form of some neural network) that learns across all data instances will typically struggle to faithfully capture this distribution. The neural-process family of models includes a variant—the latent neural process [Garnelo et al., 2018a, LNP]—that seeks to address this issue by making the encoding of the context set (originally through r_θ) a random variable. While this helps make the predictive distribution over values more flexible, it also makes learning the neural process itself harder. Furthermore, as formulated earlier, the generative model itself can be quite unwieldy as it requires defining a prior distribution over spatial arrangements of size M through $p_\theta(\mathbf{x}_M)$ —not easy to handle in a sensible fashion other than assume it is uniformly random, which is unlikely to reflect data well.

We tackle both these issue by introducing an *abstractive* latent variable a as shown in Figure 2b that serves two purposes. From the flexibility perspective, the inference model mirrors the intuition from the LNP by distilling the context set/PPS into a random variable rather than just a deterministic

value. Its role in the generative model, however, is reversed—allowing for an easier-to-define lower-dimensional latent variable prior that controls the space of possible arrangements of image pixel locations. Taken together, the latent variable \mathbf{a} acts as an abstraction of the context set/PPS, providing smooth control over different arrangements and values, while also allowing the model to flexibly learn the mapping between arrangement of pixel locations and corresponding pixel vales. The full PPS-VAE generative model can thus be defined as

$$\begin{aligned}
p_\theta(\mathbf{a}, \mathbf{x}, \mathbf{y}|M) &= p_\theta(\mathbf{a}) p_\theta(\mathbf{x}_M|\mathbf{a}) p_\theta(\mathbf{y}_M|\mathbf{x}_M, \mathbf{a}) p_\theta(\mathbf{y}_T|\mathbf{x}_T, \mathbf{x}_M, \mathbf{y}_M) \quad (2) \\
p_\theta(\mathbf{a}) &= \mathcal{N}(\mathbf{a}|\mathbf{0}, \mathbf{1}); p_\theta(\mathbf{x}_M|\mathbf{a}) = \prod_{m=1}^M GS(x_m|g_\theta^1(\mathbf{a})) \\
p_\theta(\mathbf{y}_M|\mathbf{x}_M, \mathbf{a}) &= \prod_{m=1}^M \mathcal{N}(y_m|g_\theta^2(\mathbf{x}_M, \mathbf{a})); p_\theta(\mathbf{y}_T|\mathbf{x}_T, \mathbf{x}_M, \mathbf{y}_M) = \prod_{t=1}^T \mathcal{N}(y_t|g_\theta^3(\mathbf{x}_T, \mathbf{x}_M, \mathbf{y}_M))
\end{aligned}$$

where g_θ^1 , g_θ^2 , and g_θ^3 are parametrised neural networks that transform input values to corresponding distribution parameters, and GS is the Gumbel-Softmax distribution [Maddison et al., 2017, Jang et al., 2017] which provides a continuous relaxation of the discrete distribution—enabling reparametrised gradient estimation.

To complete things, we formulate the corresponding inference model as

$$q_\phi(\mathbf{a}, \mathbf{x}_M|\mathbf{y}, M) = q_\phi(\mathbf{x}_M|\mathbf{y}) q_\phi(\mathbf{a}|\mathbf{x}_M, \mathbf{y}_M) \quad (3)$$

$$q_\phi(\mathbf{x}_M|\mathbf{y}) = \prod_{m=1}^M GS(x_m|h_\phi^1(y)) \quad (4a)$$

$$q_\phi(\mathbf{x}_M|\mathbf{y}) = \prod_{m=1}^M GS(x_m|h_\phi^2(y, x_{<m})) \quad (4b)$$

$$q_\phi(\mathbf{a}|\mathbf{x}_M, \mathbf{y}_M) = \mathcal{N}(\mathbf{a}|h_\phi^3(\mathbf{x}_M, \mathbf{y}_M)).$$

Where the generative model assumes a simple independent factorisation for $p_\theta(\mathbf{x}_M|\mathbf{a})$, the posterior typically can have varying levels of flexibility. To capture this, we explore two separate formulations of $q_\phi(\mathbf{x}_M|\mathbf{y})$ in Equations (4a) and (4b), one with an independent factorisation (PPS-VAEⁱ) and one with a more flexible autoregressive formulation (PPS-VAE^a). Again, h_ϕ^1 , h_ϕ^2 , and h_ϕ^3 are parametrised neural networks that transform inputs to distribution parameters. In PPS-VAE^a, $x_{<m}$ for $m = 1$ is assumed to be null.

Putting the generative and inference models together, we construct the variational evidence lower bound (ELBO) as

$$\begin{aligned}
\log p_\theta(\mathbf{y}|M) &\geq \mathbb{E}_{q_\phi(\mathbf{a}, \mathbf{x}_M|\mathbf{y}, M)} \left[\log \frac{p_\theta(\mathbf{a}, \mathbf{x}, \mathbf{y}|M)}{q_\phi(\mathbf{a}, \mathbf{x}_M|\mathbf{y}, M)} \right] \\
&= \mathbb{E}_{q_\phi(\mathbf{x}_M|\mathbf{y})} \log p_\theta(\mathbf{y}_T|\mathbf{x}_T, \mathbf{x}_M, \mathbf{y}_M) - D_{\text{KL}}(q_\phi(\mathbf{a}|\mathbf{x}_M, \mathbf{y}_M)||p_\theta(\mathbf{a})) \\
&\quad + \mathbb{E}_{q_\phi(\mathbf{a}|\mathbf{x}_M, \mathbf{y}_M)} [\log p_\theta(\mathbf{y}_M|\mathbf{x}_M, \mathbf{a})] - \mathbb{E}_{q_\phi(\mathbf{a}|\mathbf{x}_M, \mathbf{y}_M)} \left[\frac{q_\phi(\mathbf{x}_M|\mathbf{y})}{p_\theta(\mathbf{x}_M|\mathbf{a})} \right]
\end{aligned}$$

where \mathbf{y}_M and \mathbf{y}_T are observations derived from \mathbf{y}, \mathbf{x}_M as $\mathbf{y} \odot \mathbf{x}_M$ and $\mathbf{y} \odot \mathbf{x}_T$ respectively—lookups for complementary sets of pixel locations. Note also that the reversal of how the abstractive latent \mathbf{a} is used in the generative and inference models is reflected in the fact that an image pixel location x_m sampled from the variational posterior can only be scored in the generative model once the corresponding \mathbf{a} has been sampled. This ensures that the complex transformation involved in going from $\mathbf{x}_M \rightarrow \mathbf{y}_M$ is correctly captured by the abstractive latent. We will demonstrate its efficacy in our evaluation of unconditional generation and ability to classify from the abstractive latent directly in Sections 3.2 and 3.4.

3 Experiments

Our primary goal here is to better understand context sets/PPS. For this we, conduct four experiments. The first experiment evaluates (estimates of) the log marginal distribution (Section 3.1) to help us

Table 1: Estimated $\log p_{\theta}(\mathbf{y}|M)(\uparrow)$ for PPS-VAE^a using the IWAE estimator [Burda et al., 2015] with 1000 samples.

	FMNIST	CIFAR-10	CelebA
PPS-VAE ($M = 15$)	858	2895	10833
PPS-VAE ($M = 30$)	878	3210	12275
PPS-VAE ($M = 60$)	—	3481	—
VAE	829	3420	13573

understand how the number of points in the context set affects modelling distribution over the images. The second experiment evaluates the ability of the trained model to generate *unconditionally*—a crucial test for a generative modelling framework (Section 3.2). We wish to understand how well the latent variable a abstracts information and what kind of context sets/PPS and images it facilitates. The third experiment focusses on the encoder of PPS-VAE (Section 3.3), where the model infers context sets for the test images and we qualitatively analyse what kind of patterns are encoded in the context sets. Finally, in the fourth experiment (Section 3.4), we quantify the utility of the information encoded in our learnt representations through the lens of classification (see Appendix A). All experiments are conducted using three standard vision datasets: FashionMNIST (FMNIST), CIFAR-10 and CelebA.

Models. For all experiments we use PPS-VAE^a except for the final one where we also train PPS-VAEⁱ. We do so based on empirical results (Section 3.4.1) that indicate PPS-VAE^a strictly dominates PPS-VAEⁱ. We also find that for some datasets, a larger number of context points is needed for *qualitatively* meaningful patterns to emerge (see Section 3.3). For all the dataset we use the same M to train the models: $M = \{15, 30, 60\}$. To better ground the experimental results, we employ two standard baselines: VQ-VAE [van den Oord et al., 2017] and the vanilla VAE [Kingma and Welling, 2014]. We train all the models once and use them in all the experiments (see Appendices B,C for more details on the models).

3.1 Model Fit

Here we estimate $\log p_{\theta}(\mathbf{y}|M)$ via the importance weighted autoencoding [Burda et al., 2015, IWAE] objective (see Table 1) and use it to compare models. The first observation that we make is that for all datasets, increasing M results in better performance, which reflects the expectation that observing more context points allows to model the distribution over the images better. The second observation is that on two out of the three datasets PPS-VAE^a matches or outperforms the vanilla VAE on the metric, with the vanilla VAE doing better on CelebA. With larger M we expect PPS-VAE^a to at least match the vanilla VAE model. The comparison on numbers alone however can be misleading, as the actual vanilla VAE model is simply unable to effectively generate samples from the observed dataset (see Appendix F), whereas PPS-VAE^a does well. We do not directly compare to VQ-VAE because it doesn't directly permit estimation of the marginal likelihood—it requires a separate procedure to fit a prior. Without this, the only estimate one can do is to average the raw likelihoods of the model.

3.2 Generative Ability

We now evaluate the generative capability of PPS-VAE^a. Figure 3 (left) shows values for the intermediate variables through the generation process, and it is clear that across the different datasets, the context sets/PPS are chosen typically around object/component boundaries with a few points being chosen to capture interior colour/texture. This also demonstrates that the abstractive latent elicits reasonable arrangements of context points. For FashionMNIST and CelebA the sampled PPS does resemble objects in the datasets and the generated images do correspond to the one in the dataset. However, for CIFAR-10 things are less clear. We attribute this in part to the relatively poor resolution of objects in the dataset, which affects the ability to learn useful arrangements of PPS across the dataset (see Section 3.4) Beyond the process, we also generate multiple instances from the model to show that the samples actually reflect the diversity of data in Figure 3 (right)—for example, the type of object in FMNIST, and different attribute in CelebA; there is no mode collapse and the exemplars reflect the data well (again excepting CIFAR-10).

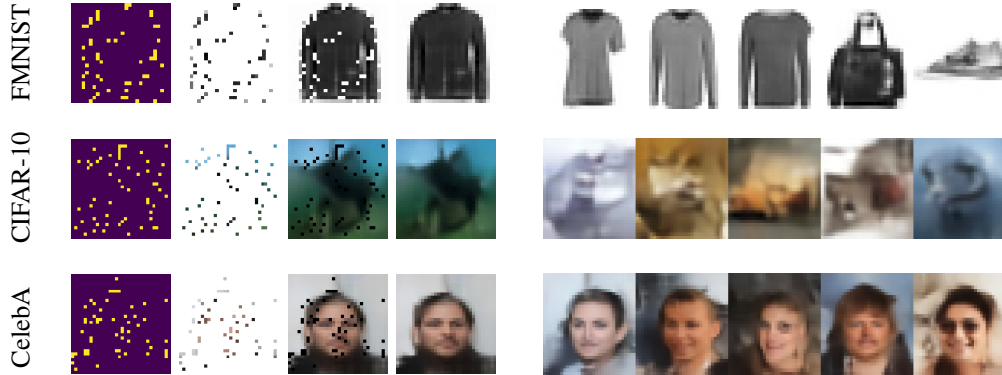


Figure 3: Unconditional generation with PPS-VAE^a. Top to bottom: FMNIST, CIFAR-10, CelebA. $M = 60$. [Left]: left to right — x_M (binary matrix, yellow colour denotes 1’s), y_M , y_T , y . [Right]: generated samples.

Table 2: FID (\downarrow) over 1000 generated images for PPS-VAE^a (FMNIST, CelebA $M = 30$; CIFAR-10 $M = 60$), with Inception-v3 (using weights from Heusel et al. [2017]).

	FMNIST	CIFAR-10	CelebA
PPS-VAE	0.21	0.91	0.82
VAE	0.35	0.73	1.53

Second we quantitatively benchmark the generated images against the vanilla VAE using FID scores [Heusel et al., 2017]³ (see Table 2). PPS-VAE^a outperforms the vanilla VAE on FID on the FashionMNIST and CelebA datasets, but not on CIFAR-10. We report the generated images of the vanilla VAE model in Appendix F.2. Note that generating samples from VQ-VAE again requires separate fitting of the prior as in Razavi et al. [2019].

3.3 PPS: Qualitative Analysis

Next, we perform a qualitative analysis of the context set/PPS inferred by the learnt PPS-VAE models on different data, for different settings of M . Results are shown in Figure 4, with additional examples given in Appendix E.1.

The patterns that context sets form can be summarised with the following three observations: 1) boundary points between objects and the background generally describe the shape, 2) points that lie on the object can be used to capture ‘interior’ colour, and part locations and 3) background points, where elicited, capture complexity outside the objects (e.g. uniform colour etc.)

We also want to emphasise that the aforementioned patterns are more pronounced when M is sufficiently large e.g. $M = 60$. This is especially true for CelebA and the CIFAR-10 datasets. However, when M relatively small compared to the complexity of an image, the context set appears scattered. A possible explanation for this is that the model tries to “cover” the complexity of the image. For example, if there are five objects in an image and $M = 5$, the model will likely prefer to assign a single point to each of the objects rather than concentrate all five points on a single object—because the former is more likely to help reconstruct the *whole* image better.

3.4 PPS: Quantitative Analysis

Having observed qualitatively that the context sets/PPS induced by PPS-VAE do indeed appear to capture meaningful features, we conduct further analyses to quantify how meaningful they can be. We do this through the lens of classification, by probing both the context set/PPS (y_M) as well as

³Using https://torchmetrics.readthedocs.io/en/stable/image/frechet_inception_distance.html

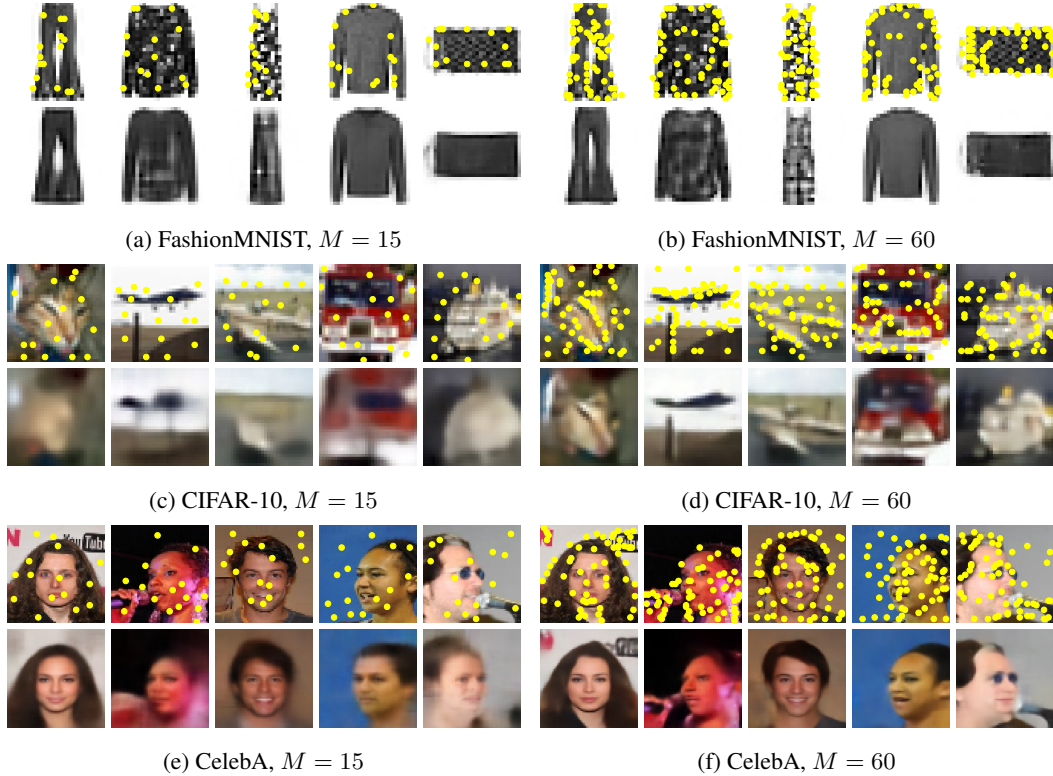


Figure 4: Visualisation of the spatial arrangement of the context set for PPS-VAE^a on three datasets: FashionMNIST (a,b) and CIFAR10 (c,d) and CelebA (f,e). In each figure [a-e] the first row corresponds to the original image, together with the inferred context set denoted by the yellow circles. The second row corresponds to the reconstructed images. The context sets are inferred on test images.

Table 3: Object classification. FMNIST: PPS-VAE/RAND ($M = 60$), VQ-VAE ($J, S = 7$). CIFAR-10: PPS-VAE/RAND ($M = 60$), VQ-VAE ($J, S = 8$). CelebA: PPS-VAE/RAND ($M = 60$), VQ-VAE ($J, S = 16$). Attr 13: Chubby, Attr 20: Male, Attr 25: Oval Face. Classifiers trained over three seeds with early stopping, reporting mean F1-macro scores. Sample means that each point in the context set was sampled, while mode means that the most probable point was selected. For PPS-VAEⁱ we only used sample as we found that mode leads to inferior performance.

		FMNIST	CIFAR-10	CelebA (Attr: 13)	CelebA (Attr: 20)	CelebA (Attr: 25)
RESNET-18	Image	94.0 ± 0.0	90.0 ± 0.0	76.3 ± 1.7	98.0 ± 0.0	66.0 ± 0.0
	PPS-RAND	79.0 ± 0.8	65.3 ± 0.5	49.0 ± 0.0	79.3 ± 0.5	42.0 ± 0.8
	VQ-VAE	89.7 ± 0.5	74.0 ± 0.0	59.0 ± 2.2	94.7 ± 0.5	58.7 ± 1.3
	PPS-VAE ³ (y_M sample)	88.0 ± 0.0	76.7 ± 0.5	50.3 ± 1.3	89.0 ± 0.0	48.0 ± 0.0
	PPS-VAE ³ (y_M mode)	89.0 ± 0.0	78.0 ± 0.0	53.0 ± 2.8	89.3 ± 0.5	53.0 ± 2.5
	PPS-VAE ⁱ (y_M sample)	86.0 ± 0.0	68.0 ± 0.0	49.0 ± 0.0	77.7 ± 0.5	41.0 ± 0.0
MLP	VAE (z)	85.3 ± 0.5	56.0 ± 0.0	49.0 ± 0.0	61.0 ± 0.8	41.0 ± 0.0
	PPS-VAE ³ (a mode)	76.0 ± 0.0	48.0 ± 0.0	49.0 ± 0.0	49.0 ± 0.8	41.0 ± 0.0
	PPS-VAE ⁱ (a sample)	77.0 ± 0.0	44.0 ± 0.0	49.0 ± 0.0	47.7 ± 0.9	41.0 ± 0.0

our abstractive latent (a) to see how well they capture class-relevant information. **NOTE:** We do not seek to achieve SOTA classification performance—that is neither our claim, nor our intention. We simply use classification as a mechanism by which we evaluate how much autoencoding a CNP results in capturing class-specific information in different variables.

PPS baselines: To evaluate the utility of the context set/PPS we find it sufficient to use y_M . Additionally employing the location variable x_M did not provide any benefits. For all the datasets we set $M = 60$. As the base classifier, we employ the Resnet-18 [He et al., 2016] architecture,

training each instance entirely from scratch. The first baseline employs the whole image \mathbf{y} (denoted Image), and is used as a yardstick to see how well a restricted context set does. The second baseline employs a random selection of context points \mathbf{y}_M (denoted PPS-RAND) to provide an indicator of how meaningful a more informative selection of context set can be. Given the discussion in Section 4 of how the VQ-VAE can be seen as a selective codebook, but without spatial meaning, we employ it as an additional baseline to see how the constraint of spatial relevance affects classification performance. Additionally, as a pre-processing step, we rescale all inputs to the Resnet-18 model (including the PPS locations) to 224×224 , and enforce them to have 3 channels. For the VQ-VAE in particular, we use an additional convolutional layer to map its latent representation to the required input shape.

Abstractive latent baselines: In Section 2 we introduce the abstractive latent variable \mathbf{a} to both allow the model to be more flexible, and to provide a better handle on controlling the distribution of possible arrangement of context sets. To test how well this latent actually captures high-level information about the image, we employ a vanilla VAE as a baseline, using its latent \mathbf{z} to classify data. The classifier employed is a simple 3-layer MLP, with the ReLU activation function.

For both types of classification, when learning, we freeze the parameters of the respective encoders, allowing only the classifier parameters to be learnt, and employ data augmentation (random crop and random horizontal flip) to regularise the model. Classifiers are optimised using the AdamW optimiser, with AmsGrad, and we report mean F1-macro.

3.4.1 Results

PPS vs. baselines: The most competitive model, relative to the performance on the classification tasks, is PPS-VAE^a. Across all datasets, PPS-VAEⁱ shows inferior performance emphasising the importance of the autoregressive factorisation of the variational posterior. Taking PPS-VAE^a for the basis of the analysis of the results (Table 3) we make the following observations. First, the arrangements of points inferred by is more indicative of the class than of PPS-RAND, which indicates that the model performs abstraction by arranging the points in a such a way to preserve the information related to class labels. Second, VQ-VAE, performs better than PPS-VAE^a only on the CelebA, while having a larger number of parameters in its latent variable than PPS-VAE^a (see Appendix J). Finally, the Resnet-18 classifier trained on the original images performs the best, which isn't too surprising since \mathbf{y} contains the original information, while VQ-VAE and PPS-VAE^a learn abstractions which may result in information loss. Overall, we see that the learned model induces context sets/PPS that does contain abstractions of the images that are useful for downstream tasks like classification, but possibly, the models are hamstrung by the choice of set size being too low to capture all the relevant information required.

\mathbf{a} vs. baselines: Classification from the abstractive latent \mathbf{a} is significantly better than chance, but still lags behind what the VAE encodes in its latent \mathbf{z} (Table 3). This is true across both the variants of the PPS-VAE. In effect, \mathbf{a} must capture information relevant to two distinct processes: first, it must provide an abstraction for the global arrangement of points in the context set \mathbf{x}_M , and second, it must contain information as to what are relevant values \mathbf{y}_M for a given arrangement of points. Conceptually, the former process will likely correlate strongly with class-specific information, but the latter is likely to muddy the water as it includes much more localised information. Intuitively also, \mathbf{a} encodes information from the context set/PPS \mathbf{y}_M , which is less information rich when compared to the whole input \mathbf{y} . The VAE on the other hand, has no such competing interests, and could construct a smoothed latent manifold from \mathbf{y} where the relevant information is appropriately arranged.

Selection of Attributes for CelebA: We selected three attributes that are generic enough to feasibly work with the relatively small number of points found in a context set. We believe this to be an important demonstration of what information a context set of size M can capture. Extending the complexity of the context sets, either in terms of direct size, or more constrained arrangements, could in principle help improve this measure.

Importance of Recurrence: As with any autoregressive model, a particular bottleneck is its computational complexity, which gets worse with increasing sequence length (M). PPS-VAE^a is no exception; and this was the motivation for PPS-VAEⁱ—to ameliorate this issue. The conditional independence allows computation in parallel, but this is likely counterbalanced by a loss of expressivity

and quality of representation. Interestingly, we find that qualitatively, it is quite difficult to identify any consistent differences in representation of the context sets/PPS (see Appendix E), however, the difference is clear when considering the quantitative performance on the downstream tasks.

4 Related Work

CNPs [Garnelo et al., 2018a] are a flexible and scalable framework for modelling distributions over functions. The framework, now more generally referred to as Neural Process Family (NPF) have seen increased popularity, with the different approaches exploring a range of features of the model. One such approach is the adaption of the CNP to properties of the data; for example, with modelling equivariances as shift equivariance [Gordon et al., 2020] and group equivariance [Kawano et al., 2021] and modeling non-Euclidean relational information [Nassar et al., 2018]. Another approach seeks improved modelling of the output dependencies between function values [Garnelo et al., 2018b]. Various other approaches exist; see Jha et al. [2022] for an extensive survey. While all such approaches explore the model’s features, to the best of our knowledge, none explore the characteristics of the context set itself. One of the primary motivations for applying CNPs in the image domain, typically expects the context set to be provided—possibly by humans—which implies that the selection of points itself is unlikely to be random.

From a representation-learning perspective, the closest to ours is the VQ-VAE [van den Oord et al., 2017]. The ability to discretise representation, and learn such a discrete ‘codebook’ through differentiable variational inference that the VQ-VAE employs, has seen successful use in more advance models such as DALL-E [Ramesh et al., 2021]. However the types of codebooks that VQ-VAE learns are not interpretable, and it typically needs additional components, such as learning a separate prior, in order to truly function as a generative model over observed data. We address both these concerns in one go by ensuring that the latent representations are interpretable, and simultaneously learn a prior that enables unconditional generation of data.

The perspective of learning latent representations/features that apply directly on the data domain, can also be compared to work that exposes *attention* mechanisms [Bahdanau et al., 2015, Mnih et al., 2014] employed for tasks. The process of inferring context points can be interpreted as a locally-restrictive way of attending to relevant parts of the image data. Specifically, such a perspective aligns best with hard attention methods [Mnih et al., 2014] as opposed to soft-attention [Bahdanau et al., 2015] by virtue of explicitly selecting particular pixels.

Furthermore, inferring context points can also be viewed as a variant of Masked Image Modeling [Pathak et al., 2016, MIM]. MIM involves learning models and representation in a self-supervised fashion by masking parts of an image, and attempting to impute them. More recently, this has been studied extensively as masked autoencoders [He et al., 2022, MAE]. The imputation task itself is strongly connected to what CNPs do, and one could ask a similar question of MIMs that we ask of CNPs: what kinds of masks do MIMs like to impute? In fact such a question was indeed asked in work by Shi et al. [2022, ADIOS] who learnt masks simultaneously with a feature extractor in an adversarial fashion. This however, is not generative, and as with as masking-based approaches, involves complications with how to specify and generate masks in a sensible manner. A key distinction is in terms of the sparsity of observed data—MIM and related approaches typically imputes a small part of the image, where CNPs have a more complex task given sparse input. PPS-VAE employs context points as weak specifiers of which parts of the image to contextualise, leaving to the CNP itself the question of how to use that specification to capture relevant local and global information from the data.

5 Conclusion

Here, we presented PPS-VAE, a novel VAE framework that allows us to infer context sets for conditional neural processes (CNPs). We formulate our models and evaluate them across multiple vision datasets, while exploring the utility of learning context sets directly in an unsupervised manner. We observe that with the appropriate inductive biases and latent variables, the model is able to induce context sets that are visually meaningful, evaluated through both qualitative and quantitative means. To various degrees, the arrangement of pixel locations and values in the context set encode

information about the objects in the image (classification), indicating that the framework has promise as a model for learning meaningful representations of data.

6 Limitations

We would like to outline a number of limitation the present framework has:

- Interpretability of the context set is limited. To improve it, instead of inferring a single location, a more interpretable encoder could capture M ‘closed’ regions. This would allow us to compare against the slot-attention models such as [Locatello et al. \[2020\]](#).
- The form of information captured by the abstractive latent variable a .
- Exploration of inductive biases, and modelling updates would be interesting avenues to see if the latent variable can capture relevant information more cleanly.

Acknowledgments and Disclosure of Funding

The authors gratefully acknowledge the support of ELIAI (The Edinburgh Laboratory for Integrated Artificial Intelligence) EPSRC (grant no EP/W002876/1). Ivan Titov also acknowledges Dutch National Science Foundation (NWO Vici VI.C.212.053).

References

- D. Bahdanau, K. Cho, and Y. Bengio. Neural machine translation by jointly learning to align and translate. In *International Conference on Learning Representations (ICLR)*, 2015.
- Y. Burda, R. Grosse, and R. Salakhutdinov. Importance weighted autoencoders. In *International Conference on Learning Representations*, 2015.
- C. Conwell and T. Ullman. Testing relational understanding in text-guided image generation, 2022.
- W. Feng, X. He, T.-J. Fu, V. Jampani, A. Akula, P. Narayana, S. Basu, X. E. Wang, and W. Y. Wang. Training-free structured diffusion guidance for compositional text-to-image synthesis, 2023.
- M. Garnelo, D. Rosenbaum, C. Maddison, T. Ramalho, D. Saxton, M. Shanahan, Y. W. Teh, D. J. Rezende, and S. M. A. Eslami. Conditional neural processes. In *International Conference on Machine Learning (ICML)*, volume 80 of *Proceedings of Machine Learning Research*, pages 1690–1699, 2018a.
- M. Garnelo, J. Schwarz, D. Rosenbaum, F. Viola, D. J. Rezende, S. M. A. Eslami, and Y. W. Teh. Neural processes. *CoRR*, abs/1807.01622, 2018b.
- X. Glorot and Y. Bengio. Understanding the difficulty of training deep feedforward neural networks. In Y. W. Teh and M. Titterton, editors, *Proceedings of the Thirteenth International Conference on Artificial Intelligence and Statistics*, volume 9 of *Proceedings of Machine Learning Research*, pages 249–256, Chia Laguna Resort, Sardinia, Italy, 13–15 May 2010. PMLR. URL <https://proceedings.mlr.press/v9/glorot10a.html>.
- J. Gordon, W. P. Bruinsma, A. Y. K. Foong, J. Requeima, Y. Dubois, and R. E. Turner. Convolutional conditional neural processes. In *International Conference on Learning Representations (ICLR)*, 2020.
- K. He, X. Zhang, S. Ren, and J. Sun. Deep residual learning for image recognition. In *Conference on Computer Vision and Pattern Recognition (CVPR)*, pages 770–778, 2016.
- K. He, X. Chen, S. Xie, Y. Li, P. Dollár, and R. Girshick. Masked autoencoders are scalable vision learners. In *Proceedings of the IEEE/CVF Conference on Computer Vision and Pattern Recognition*, pages 16000–16009, 2022.
- M. Heusel, H. Ramsauer, T. Unterthiner, B. Nessler, and S. Hochreiter. Gans trained by a two time-scale update rule converge to a local nash equilibrium. In I. Guyon, U. V. Luxburg, S. Bengio, H. Wallach, R. Fergus, S. Vishwanathan, and R. Garnett, editors, *Advances in Neural Information Processing Systems*, volume 30. Curran Associates, Inc., 2017. URL <https://proceedings.neurips.cc/paper/2017/file/8a1d694707eb0fefe65871369074926d-Paper.pdf>.

- E. Jang, S. Gu, and B. Poole. Categorical reparameterization with gumbel-softmax. In *International Conference on Learning Representations (ICLR)*, 2017.
- S. Jha, D. Gong, X. Wang, R. E. Turner, and L. Yao. The neural process family: Survey, applications and perspectives, 2022.
- M. Kawano, W. Kumagai, A. Sannai, Y. Iwasawa, and Y. Matsuo. Group equivariant conditional neural processes. In *International Conference on Learning Representations (ICLR)*, 2021.
- D. P. Kingma and M. Welling. Auto-encoding variational bayes. In *International Conference on Learning Representations (ICLR)*, 2014.
- A. Krizhevsky and G. Hinton. Learning multiple layers of features from tiny images. Technical report, University of Toronto, 2009.
- Z. Liu, P. Luo, X. Wang, and X. Tang. Deep learning face attributes in the wild. In *International Conference on Computer Vision (ICCV)*, pages 3730–3738, 2015.
- Z. Liu, H. Mao, C.-Y. Wu, C. Feichtenhofer, T. Darrell, and S. Xie. A convnet for the 2020s. 2022.
- F. Locatello, D. Weissenborn, T. Unterthiner, A. Mahendran, G. Heigold, J. Uszkoreit, A. Dosovitskiy, and T. Kipf. Object-centric learning with slot attention, 2020.
- I. Loshchilov and F. Hutter. Decoupled weight decay regularization. In *International Conference on Learning Representations (ICLR)*, 2019.
- C. J. Maddison, A. Mnih, and Y. W. Teh. The concrete distribution: A continuous relaxation of discrete random variables. In *International Conference on Learning Representations (ICLR)*, 2017.
- V. Mnih, N. Heess, A. Graves, and K. Kavukcuoglu. Recurrent models of visual attention. In *Advances in Neural Information Processing Systems (NeurIPS)*, pages 2204–2212, 2014.
- M. Nassar, X. Wang, and E. Tumer. Conditional graph neural processes: A functional autoencoder approach. *Third Workshop on Bayesian Deep Learning (NeurIPS 2018)*, abs/1812.05212, 2018.
- D. Pathak, P. Krähenbühl, J. Donahue, T. Darrell, and A. A. Efros. Context encoders: Feature learning by inpainting. In *Conference on Computer Vision and Pattern Recognition (CVPR)*, pages 2536–2544, 2016.
- A. Ramesh, M. Pavlov, G. Goh, S. Gray, C. Voss, A. Radford, M. Chen, and I. Sutskever. Zero-shot text-to-image generation. In *International Conference on Machine Learning (ICML)*, volume 139 of *Proceedings of Machine Learning Research*, pages 8821–8831, 2021.
- A. Razavi, A. van den Oord, and O. Vinyals. *Generating Diverse High-Fidelity Images with VQ-VAE-2*. Curran Associates Inc., Red Hook, NY, USA, 2019.
- S. J. Reddi, S. Kale, and S. Kumar. On the convergence of adam and beyond. In *International Conference on Learning Representations (ICLR)*, 2018.
- Y. Shi, N. Siddharth, P. H. Torr, and A. R. Kosiorek. Adversarial masking for self-supervised learning. In *International Conference on Machine Learning (ICML)*, 2022.
- A. van den Oord, O. Vinyals, and K. Kavukcuoglu. Neural discrete representation learning. In *Advances in Neural Information Processing Systems (NeurIPS)*, pages 6306–6315, 2017.
- H. Xiao, K. Rasul, and R. Vollgraf. Fashion-mnist: a novel image dataset for benchmarking machine learning algorithms, 2017. URL <https://arxiv.org/abs/1708.07747>.
- M. Zaheer, S. Kottur, S. Ravanbakhsh, B. Póczos, R. Salakhutdinov, and A. J. Smola. Deep sets. In *Advances in Neural Information Processing Systems (NeurIPS)*, pages 3391–3401, 2017.

A Datasets

FashionMNIST comprises of 60K training and 10K test 28x28 grayscale images of cloth. Overall there are 10 classes of cloth: such as trousers, boots, jackets etc. CIFAR10 consist of 50K training and 10K test 32x32 colored images of objects from 10 classes: airplane, bird, frog etc. Finally, CelebA consist of ≈ 163 K training and ≈ 20 K test face images with various attributes. We resize each image (for CelebA) to 64x64. We perform the classification on the three attributes: male, oval face and chubby. We renormalise the pixel values of the images, from all the datasets, to be on the scale $[0, 1]$.

B Implementation and Training of PPS-VAE

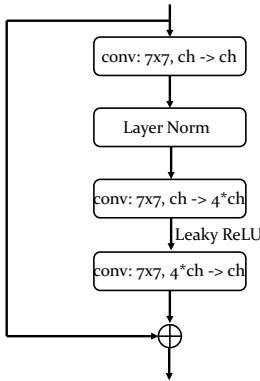


Figure 5: A schematic of ConvNetXt used. ch - corresponds to the number channels.

We parameterise the PPS-VAE with CNN neural networks. More concretely, we use convolutional blocks similar to ConvNetXt [Liu et al., 2022], with *Leaky ReLU* activation function (see Figure 5). We found that with *GELU* activation function training of PPS-VAE can be unstable. Also, we do not decrease the HxW dimensions of the original image, hence the induced $x_{1:M} \in \{0, 1\}^{B \times H \times W \times 1}$ and $y_{1:M} \in [0, 1]^{B \times H \times W \times C}$, where B is the batch size. However, we represent the latent variable a in a vector such that $a \in \mathbb{R}^{B \times D}$. We set D to be 32, however any other values would work. Moreover, to model distributions such as $p_{\theta}(y_{1:M} | x_{1:M}, a)$ we concatenate $x_{1:M}$ and a along the channel dimension. For this we map a from $a \in \mathbb{R}^{B \times D}$ to $a \in \mathbb{R}^{B \times H \times W \times D}$.

We optimise the parameters of the model with the AdamW [Loshchilov and Hutter, 2019] optimiser, setting the learning rate to $2 * 10^{-4}$ and we also enable the amsgrad [Reddi et al., 2018]. We train the PPS-VAE with the autoregressive posterior (PPS-VAE^a) for 200 epochs and the PPS-VAE with the independent posterior (PPS-VAEⁱ) for 400 epochs. This is sufficient for the models to converge on the aforementioned datasets.

C Baseline Models

C.1 VAE

The encoder of the vanilla VAE baseline comprises of eight convolutional layers: 3 are the vanilla convolutions and 3 ConvNetXt blocks and 2 vanilla convolutions to model the mean and variance of the variational posterior distribution, which is Gaussian. Both the mean and the variance are 256 dimensional vectors. Decoder comprises of transposed convolutions with *Leaky ReLU* activation function inserted between them. We optimise the parameters of the model with the AdamW optimiser, setting the learning rate to $2 * 10^{-4}$ and we also enable the amsgrad.

C.2 VQVAE

The encoder of the VQVAE comprises of the 2 vanilla convolutional layers and 2 ResNet blocks. The decoder comprises of the 2 ResNet blocks and two transposed convolutions. As between the

layers we insert *ReLU* activation function. The codebook is initialised with the *xavier uniform* initialiser [Glorot and Bengio \[2010\]](#). The latent representation of an image $z \in \mathbb{R}^{B \times J \times S \times D}$, where J and S are the reduced height and width of the original image and D , which we set to 64, is the dimensionality of the vectors in the codebook. For each of the datasets the number of the vectors in the codebook matches M of the PPS-VAE model. That is for FashionMNIST, CelebA and CIFAR10 there are 60 vectors in the codebook. We optimise the parameters of the model with the AdamW optimiser, setting the learning rate to $3 * 10^{-4}$ and we also enable the amsgrad.

D PPS-VAE^a

D.1 Inference: Context Set

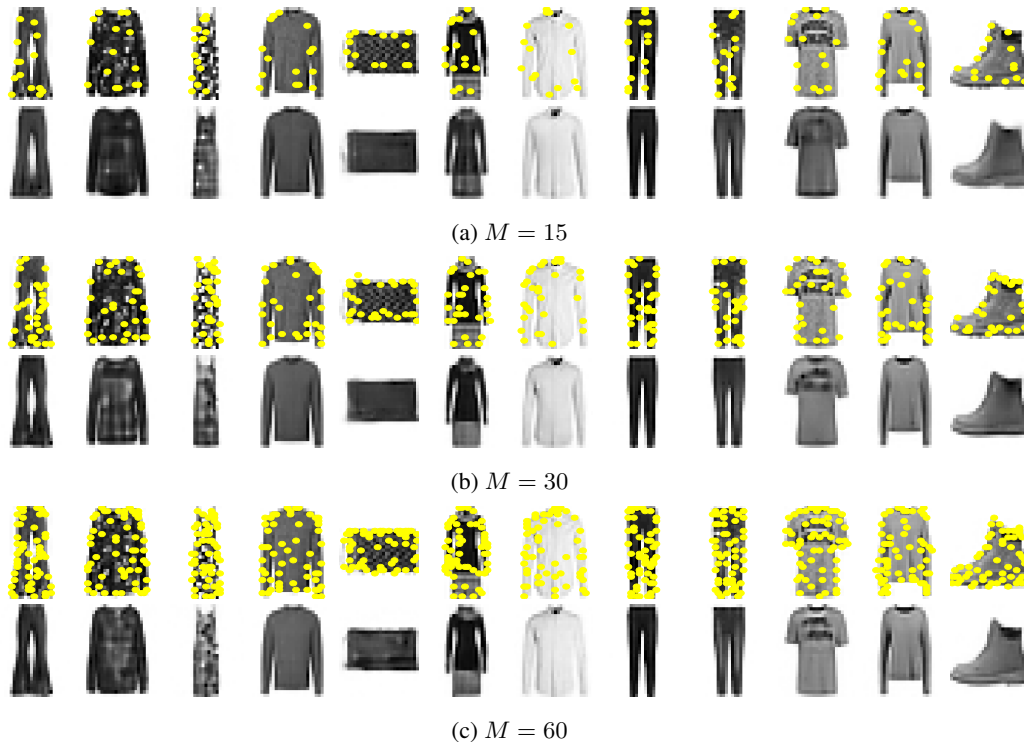
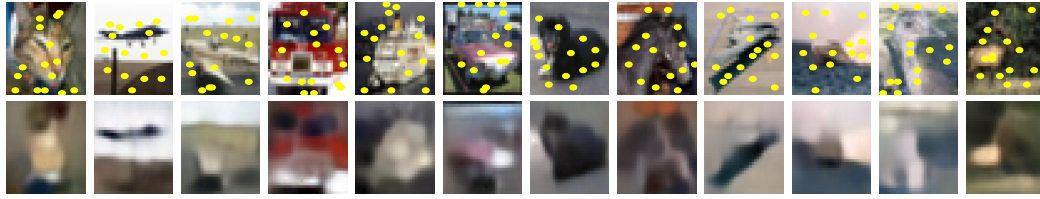
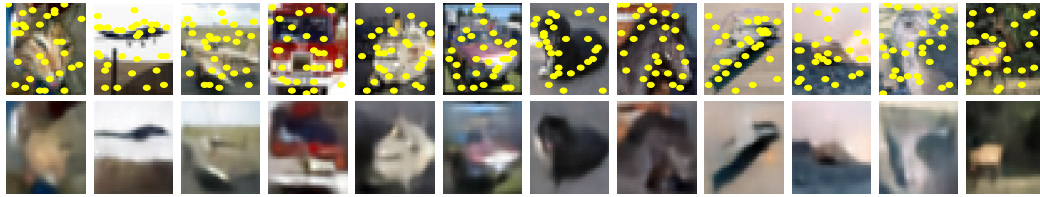


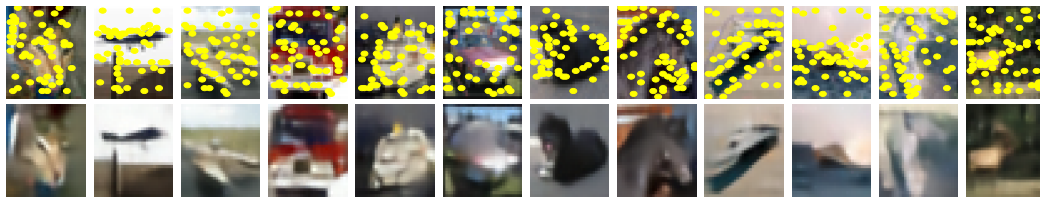
Figure 6: Visualisation of the spatial arrangement of points in the context sets (PPS-VAE^a) — conducted on the FashionMNIST dataset. The first row corresponds to the original image, together with the inferred context set denoted by the yellow circles. The second row corresponds to the reconstructed images. The context sets inferred on the test images.



(a) $M = 15$

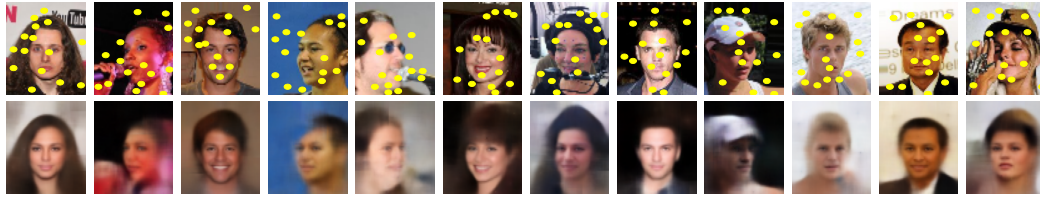


(b) $M = 30$

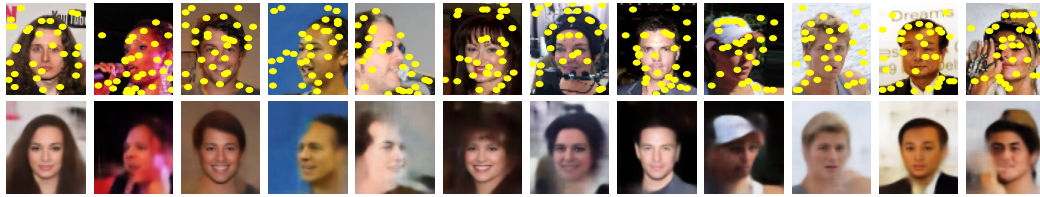


(c) $M = 60$

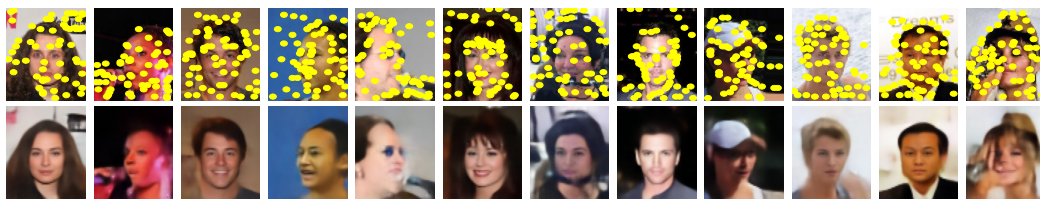
Figure 7: Visualisation of the spatial arrangement of points in the context sets (PPS-VAE^a) — conducted on the CIFAR-10 dataset. The first row corresponds to the original image, together with the inferred context set denoted by the yellow circles. The second row corresponds to the reconstructed images. The context sets inferred on the test images.



(a) $M = 15$



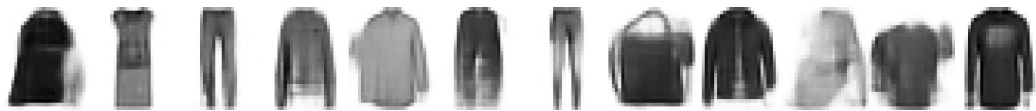
(b) $M = 30$



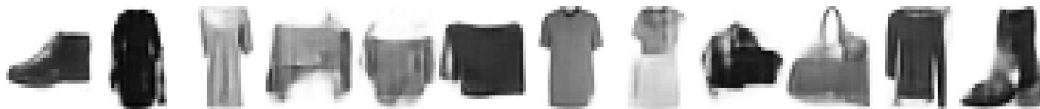
(c) $M = 60$

Figure 8: Visualisation of the spatial arrangement of points in the context sets (PPS-VAE^a) — conducted on the CelebA dataset. The first row corresponds to the original image, together with the inferred context set denoted by the yellow circles. The second row corresponds to the reconstructed images. The context sets inferred on the test images.

D.2 Unconditional Generation: Context Set



(a) $M = 15$

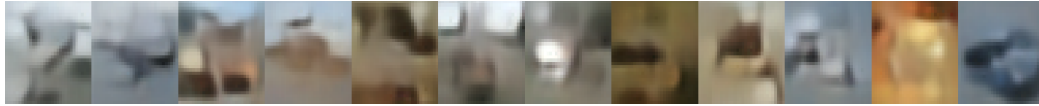


(b) $M = 30$

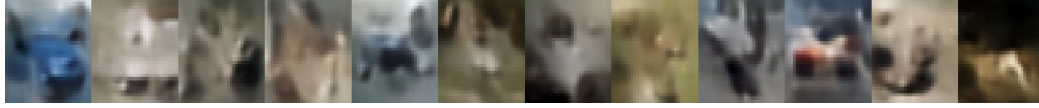


(c) $M = 60$

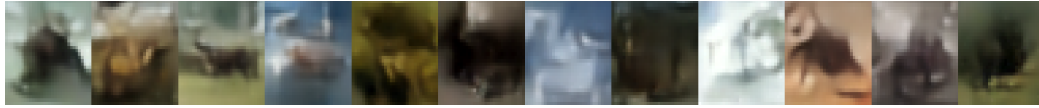
Figure 9: Images generated by the PPS-VAE^a model. FashionMNIST dataset.



(a) $M = 15$

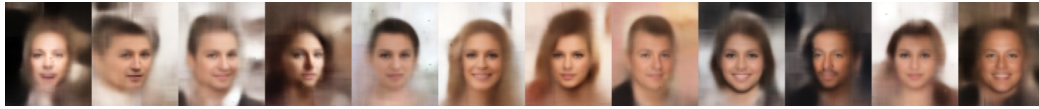


(b) $M = 30$

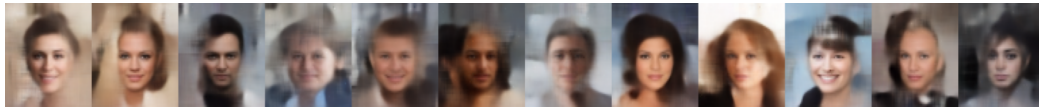


(c) $M = 60$

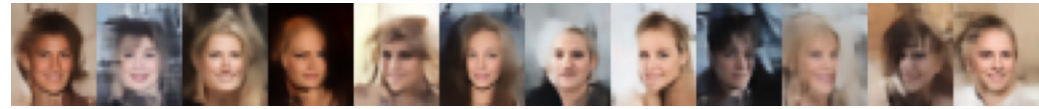
Figure 10: Images generated by the PPS-VAE^a model. CIFAR-10 dataset.



(a) $M = 15$



(b) $M = 30$



(c) $M = 60$

Figure 11: Images generated by the PPS-VAE^a model. CelebA dataset.

E PPS-VAEⁱ

E.1 Inference: Context Set

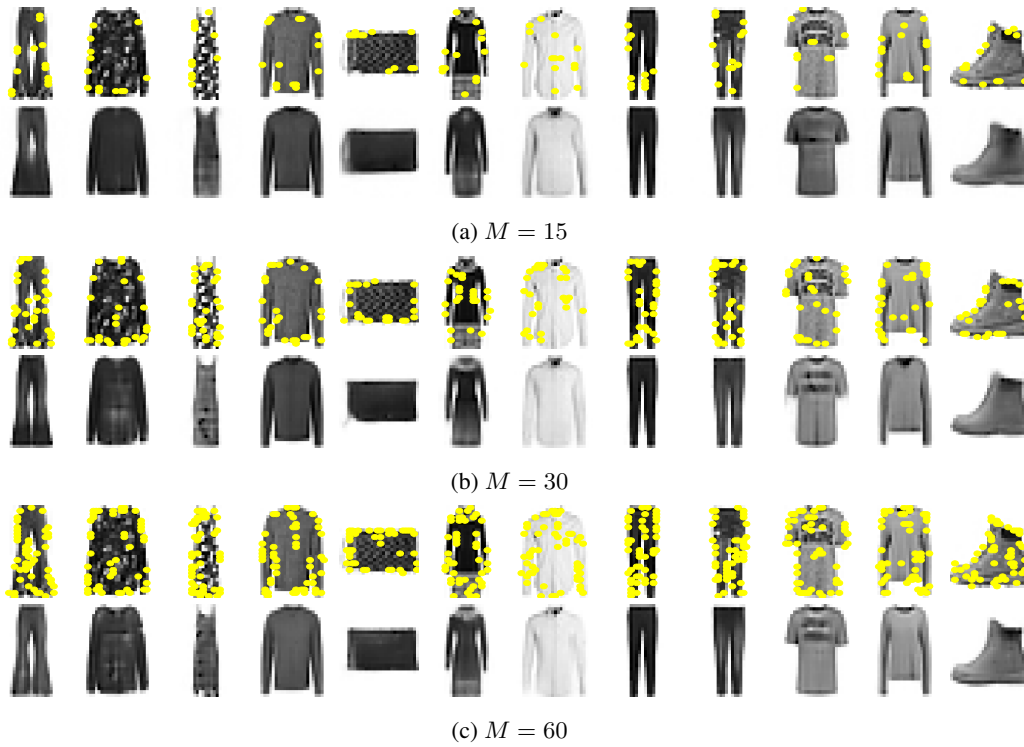
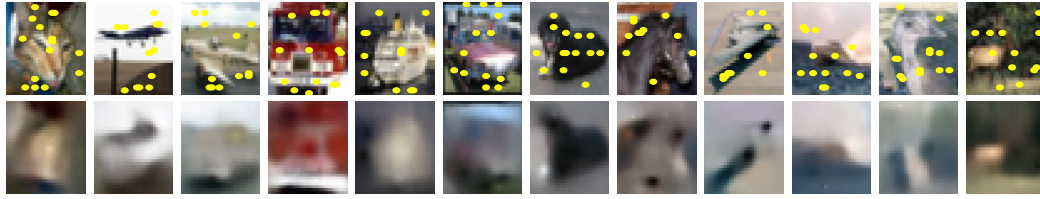
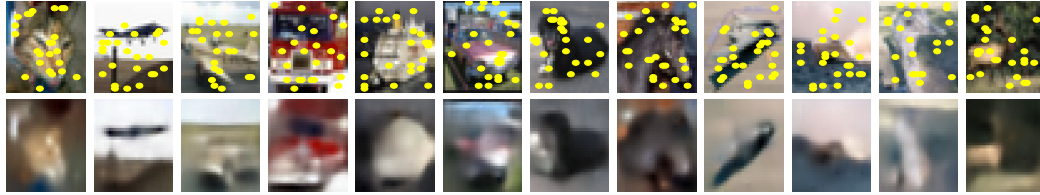


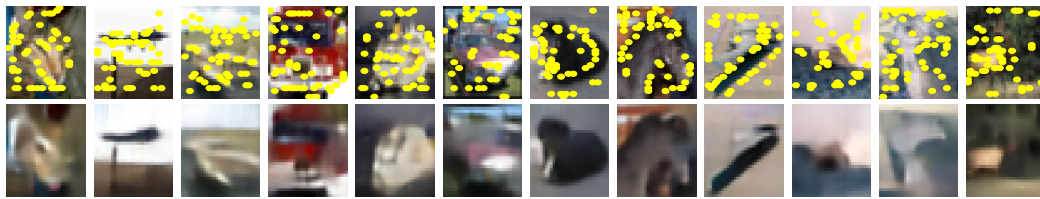
Figure 12: Visualisation of the spatial arrangement of points in the context sets (PPS-VAEⁱ) — conducted on the FashionMNIST dataset. The first row corresponds to the original image, together with the inferred context set denoted by the yellow circles. The second row corresponds to the reconstructed images. The context sets inferred on the test images.



(a) $M = 15$

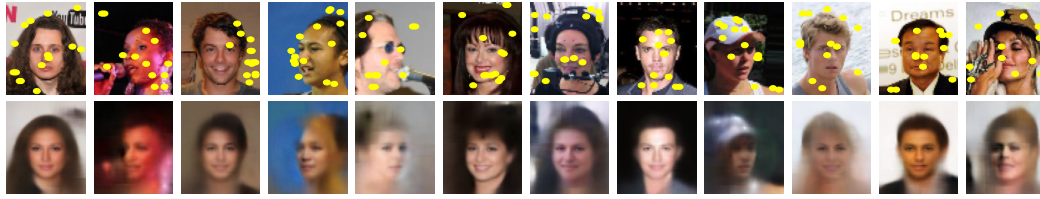


(b) $M = 30$

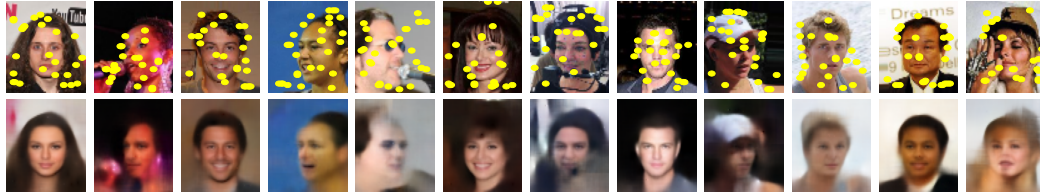


(c) $M = 60$

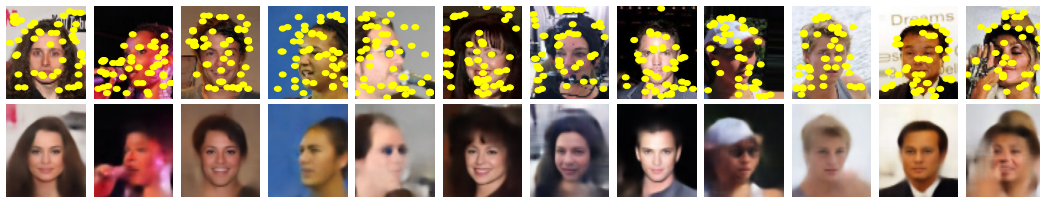
Figure 13: Visualisation of the spatial arrangement of points in the context sets (PPS-VAE¹) — conducted on the CIFAR-10 dataset. The first row corresponds to the original image, together with the inferred context set denoted by the yellow circles. The second row corresponds to the reconstructed images. The context sets inferred on the test images.



(a) $M = 15$



(b) $M = 30$



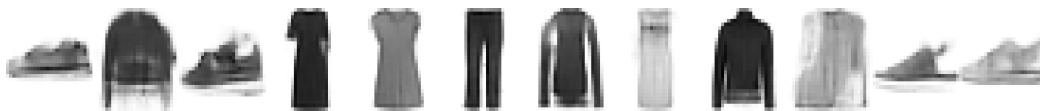
(c) $M = 60$

Figure 14: Visualisation of the spatial arrangement of points in the context sets (PPS-VAEⁱ) — conducted on the CelebA dataset. The first row corresponds to the original image, together with the inferred context set denoted by the yellow circles. The second row corresponds to the reconstructed images. The context sets inferred on the test images.

E.2 Unconditional Generation: Context Set



(a) $M = 15$



(b) $M = 30$

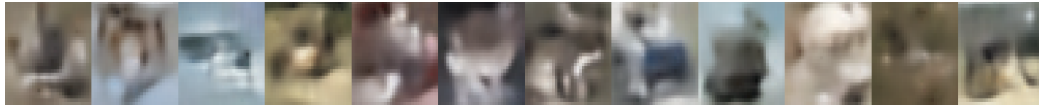


(c) $M = 60$

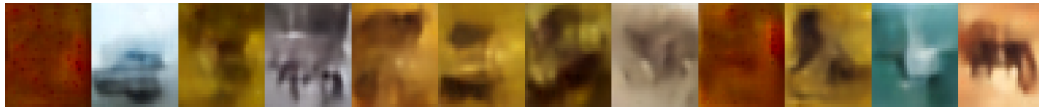
Figure 15: Images generated by the PPS-VAEⁱ model. FashionMNIST dataset.



(a) $M = 15$

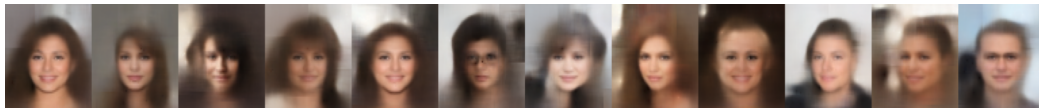


(b) $M = 30$

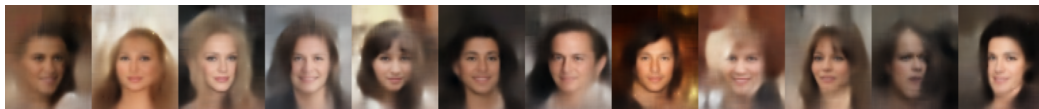


(c) $M = 60$

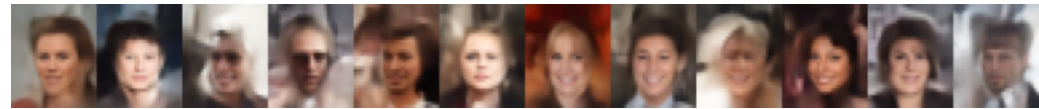
Figure 16: Images generated by the PPS-VAEⁱ model. CIFAR-10 dataset. CelebA dataset.



(a) $M = 15$



(b) $M = 30$



(c) $M = 60$

Figure 17: Images generated by the PPS-VAEⁱ model.

F Vanilla VAE

F.1 Reconstruction

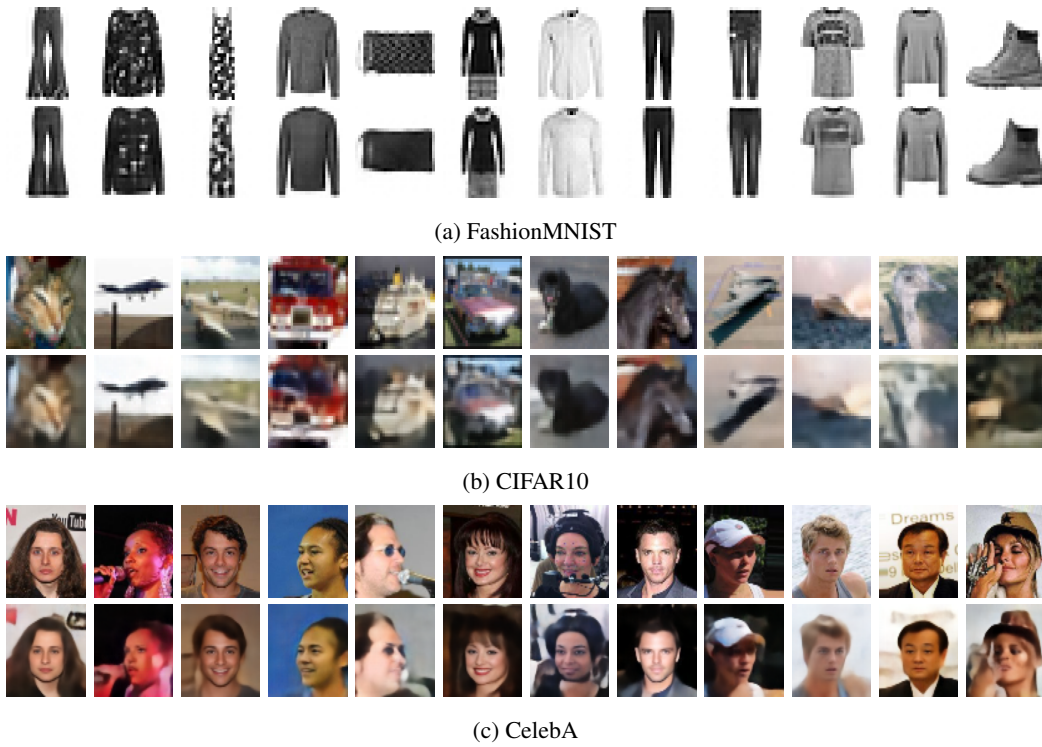


Figure 18: Images reconstructed by the vanilla vae model. The first row corresponds to the original image. The second row corresponds to the reconstructed images.

F.2 Unconditional Generation



Figure 19: Images generated by vanilla vae model.

G VQ-VAE

G.1 Reconstruction

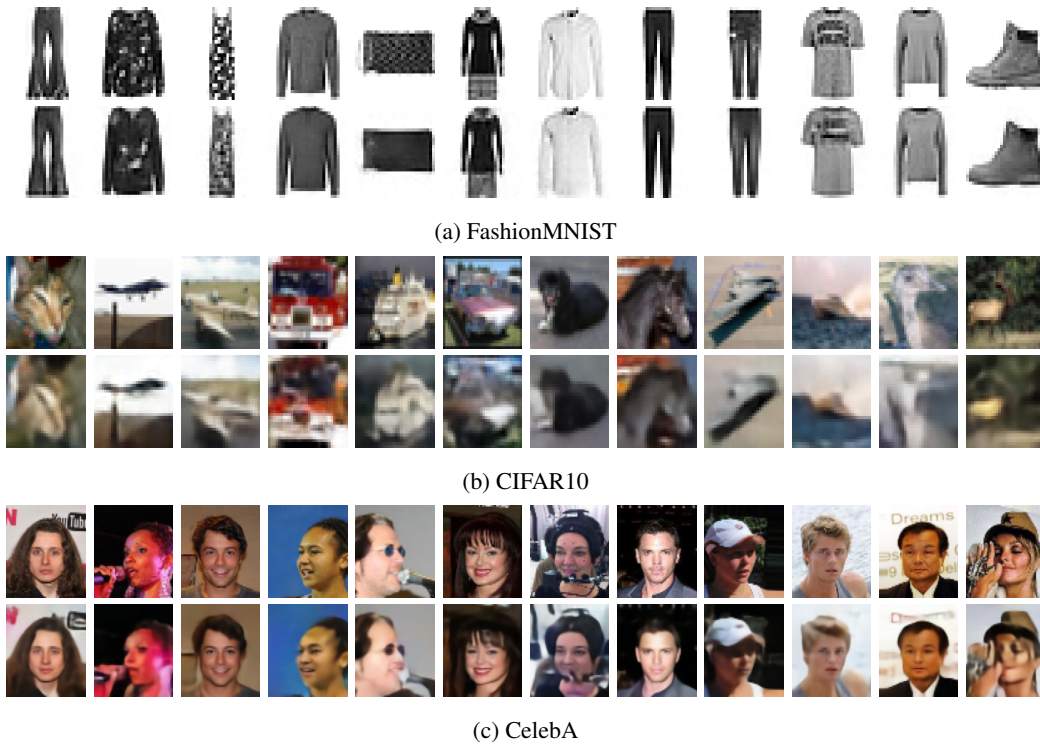


Figure 20: Images reconstructed by the VQ-VAE model. The first row corresponds to the original images. The second row corresponds to the reconstructed images.

H Classification Results: Number of Points in Context Sets vs Classification Performance

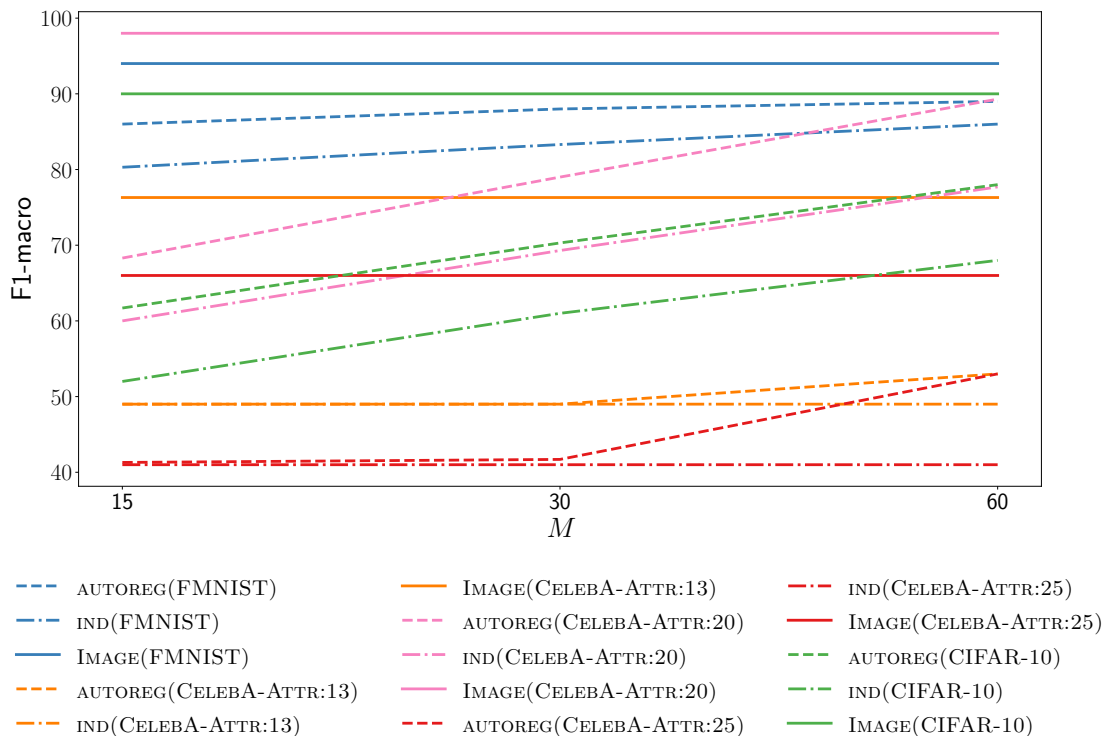
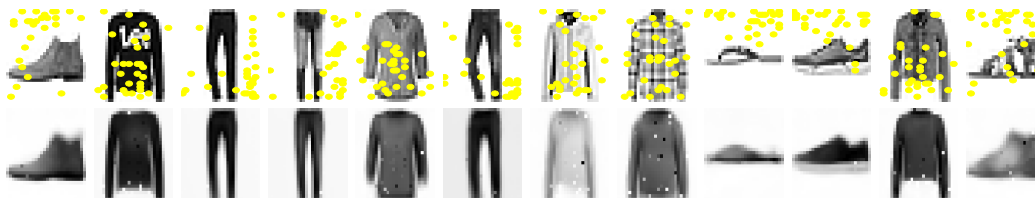


Figure 21: The Resnet-18 F1-macro on y_M for various $M = \{15, 30, 60\}$. We train both PPS-VAE^a (AUTOREG) and PPS-VAEⁱ (IND). Image: Resnet-18 trained on whole image y .

I Inductive Bias: MLP CNP

In the earlier version of the PPS-VAE model, we found that the parametrisation of the model with MLP layers as in [Garnelo et al. \[2018a\]](#) may bias the model to infer points around the edges of an image (see Figure 22a).



(a) $M = 30$

Figure 22: Visualisation of the spatial arrangement of points in the context sets for the CNP decoder parameterised by the MLP — conducted on the FashionMNIST dataset. The first row corresponds to the original image, together with the inferred context set denoted by the yellow circles. The second row corresponds to the reconstructed images. The context sets inferred on the test images.

J Number of Parameters in the Models

Table 4: Number of parameters in a model. PPS-VAE (M = 60): FMNIST, CelebA, CIFAR-10.

	FMNIST	CIFAR-10	CelebA
PPS-VAE ^a	7,079,617	7,606,761	13,357,545
PPS-VAE ⁱ	7,081,532	7,608,676	13,359,460
VAE	11,640,017	13,684,931	39,646,403
VQ-VAE	9,353,633	9,370,019	9,370,019

To calculate total number of parameters in the model we use:

```
params = sum(p.numel() for p in model.parameters() if p.requires_grad)
```

J.1 Number of Parameters in the Latent PPS-VAE vs VQ-VAE

The latent variable of VQ-VAE has the following number of parameters: FashionMNIST – $7*7*32$, CIFAR-10 – $8*8*32$ and CelebA – $16*16*32$. We calculated the number of latents by $J * S * D$. While for the context set that is: FashionMNIST – $60*(1+1)$, CIFAR-10 – $60*(3+1)$ and CelebA – $60*(3+1)$.

K Compute

We run each experiment using the hardware specified in Table 5.

Table 5: Computing infrastructure.

hardware	specification
CPU	AMD [®] EPYC 7413 24-Core Processor
GPU	NVIDIA [®] A40 x 1

L Broader Impacts

The work we describe in this paper aims to improve the interpretability of the latent representations. We foresee that further development of the described algorithm may allow to overcome a number of drawbacks of Deep Generative Models (DGMs) e.g. [Feng et al. \[2023\]](#), [Conwell and Ullman \[2022\]](#) by addressing these issues at the representation level (e.g. by explicit manipulation of latent representations to rectify mistakes DGMs). However, the current work is algorithmic in nature. And at present stage is not tied to particular applications, let alone deployments.

M Algorithm

Algorithm 1 PPS-VAE (autoregressive posterior)

```
// ** Inference **  
Input:  $y \in \mathbb{R}^{C \times H \times W}$   
Initialize  $x_0 \in \{0, 1\}^{C \times H \times W} = 0$ ,  $x_{1:M} = [x_0]$   
for  $i = 1$  to  $M$  do  
     $x_i \sim q_\phi(x_i | y, x_{1:M}[0 : i])$   
     $x_{1:M}.append(x_i)$   
end for  
 $x_{1:M} = \text{sum}(x_{1:M}, \text{axis} = 0) \in \{0, 1\}^{1 \times H \times W}$   
// points can be sampled twice, remove duplicates  
 $x_{1:M} = x_{1:M} / x_{1:M}$   
 $y_{1:M} = y * x_{1:M}$   
 $a \sim q_\phi(a | x_{1:M}, y_{1:M})$   
// ** Scoring **  
 $\text{loss}(x_{1:M}) = \log q_\phi(x_{1:M} | y) - \log p_\theta(x_{1:M} | a)$   
 $\text{loss}(a) = KL[q_\phi(a | y_{1:M}, x_{1:M}) || p_\theta(a)]$   
// get the target variables  
 $x_{1:T} = 1 - x_{1:M}$ ,  $y_{1:T} = y * x_{1:T}$   
 $\text{loss}(y_{1:M}) = \log p_\theta(y_{1:M} | x_{1:M}, a)$   
 $\text{loss}(y_{1:T}) = \log p_\theta(y_{1:T} | y_{1:M}, x_{1:M}; x_{1:T})$ 
```
